Supplementary Materials: Study of Cathode Materials for Lithium-Ion Batteries: Recent Progress and New Challenges

Florian Schipper,[a] Prasant Kumar Nayak,[a] Evan M. Erickson,[a] S. Francis Amalraj,[a] Onit Srur-Lavi,[a] Tirupathi Rao Penki,[a] Michael Talianker,[b] Judith Grinblat,[a] Hadar Sclar,[a] Ortal Breur,[a] Christian M. Julien,[c] Nookala Munichandraiah,[d] Daniela Kovacheva,[e] Mudit Dixit,[a] Dan Thomas Major,[a] Boris Markovsky,[a] Doron Aurbach[a*]

[a]*Department of Chemistry, Bar-Ilan University, Ramat Gan 5290002, Israel*

[b]*Department of Materials Engineering, Ben-Gurion University of the Negev, Beer Sheva 84105, Israel*

[c]*Sorbonne Universités, The Phénix Operation, UPMC — Université Pierre et Marie Curie — Paris 6, 75252 Paris cedex 05, France*

[d]*Department of Inorganic and Physical Chemistry, Indian Institute of Science, Bangalore-560012, India*

[e]*Institute of General and Inorganic Chemistry, Bulgarian Academy of Sciences, Sofia 1113, Bulgaria*

1. Lithium- and Manganese-Rich Layered-Structure Materials

Table S1. Literature Survey of Li- and Mn-Rich Porous Cathode Materials for LIBs

S. No.	Composition and porous morphology	Synthetic route	Rate capability mAh g^{-1} – C rate (current density = mA g^{-1})	Ref.
1	$Li_{1.2}Ni_{0.13}Mn_{0.54}Co_{0.13}O_2$ hierarchically porous microrod	Hydrothermal method	280.7-0.1 C, 254.8-0.2 C, 232.3-0.5 C, 225.6-1 C, 201.7-2 C, 172.7-5 C	[1]
2	$Li_{1.2}Ni_{0.2}Mn_{0.6}O_2$ Hierarchical Nano–Micro spherical	PVP-hydrothermal method	283.1-0.1 C, 257.5-0.2 C, 239.9-0.5 C, 209.4-1 C, 185.8-2 C, 122.6-5 C	[2]
3	$Li_{1.2}Mn_{0.56}Ni_{0.12}Co_{0.12}O_2$	Solvothermal method	292.3-0.2 C, 257-0.5 C, 229.7- 1.0 C, 183.2-2.0 C, 161.1 -5.0 C, 131.1-10 C	[3]
4	$0.5Li_2MnO_3 \cdot 0.5LiMn_{0.4}Co_{0.3}Ni_{0.3}O_2$ Hollow Porous Hierarchical-Structured	Solvothermal method	296.5-0.2 C, 270.6- 0.5 C, 243.6-1 C , 207.8-3 C, 187.4-5 C	[4]
5	$Li[Li_{0.2}Ni_{0.2}Mn_{0.6}]O_2$ Hierarchical Morphology	One-pot resorcinol formaldehyde method	241mAh g^{-1}- 50 mA g^{-1}, 160 mAh g^{-1}-1600 mA g^{-1}	[5]
6	$Li_{1.2}Ni_{0.2}Mn_{0.6}O_2$ hierarchical micro/nano	hydrothermal method	281.4,-0.1 C, 252.1-0.2 C, 238.4-0.5 C, 217.4-1 C, 180.1-2 C, 157.9-5 C	[6]
7	$Li_{1.165}Mn_{0.501}Ni_{0.167}Co_{0.167}O_2$	Ultrasonic-assisted co-precipitation method	276.6 mAh g^{-1} at 0.1 C, 60.5 mAh g^{-1} at 10 C	[7]
8	Mesoporous $0.4Li_2MnO_3:0.6LiNi_{2/3}Mn_{1/3}O_2$	gel-combustion method	291 mA h g^{-1} 115 mA g^{-1}, 208 mA h g^{-1}. 200 mA g^{-1},	[8]
9	Macroporous $Li_{1.2}Mn_{0.54}Ni_{0.13}Co_{0.13}O_2$	Aerogel template	284.2-20 mA g^{-1}, 230.8-40 mA g^{-1} 221.2-100 mA g^{-1}, 207.4-200 mA g^{-1} 192.0-400 mA g^{-1},170-1000 mA g^{-1},150- 2000 mA g^{-1}	[9]
10	$Li_{1.2}Mn_{0.53}Ni_{0.13}Co_{0.13}O_2$	Reverse microemulsion method employing a soft polymer template	250 mAh g^{-1}- 40 mAh g^{-1} 110 mAh g^{-1}- 1000 mAh g^{-1}	[10]
11	$Li_{1.2}Mn_{0.54}Ni_{0.22}Fe_{0.04}O_2$	Inverse microemulsion method	186 mAh g^{-1}- 25 mA g^{-1}. 40 mAh g^{-1}- 622 mA g^{-1}.	[11]
12	$Li[Li_{0.19}Mn_{0.32}Co_{0.49}]O_2$,	Oxalates co-crystallization in reverse micellar microemulsion	267mAh g^{-1} at 0.2 C, 209.5mAh g^{-1}-1 C, 145.4mAh g^{-1},-5C	[12]
13	$0.5Li_2MnO_3:0.5LiMn_{1/3}Ni_{1/3}Co_{1/3}O_2$	Co-precipitation of metal oxalates with an assistance of a moderate polyethylene glycol (PEG2000).	262 mAh g^{-1} at 0.1 C, 135 mAh g^{-1} at 4 C,	[13]
14	$Li_{1.2}Ni_{0.13}Co_{0.13}Mn_{0.54}O_2$ microspheres	Urea-assisted combustion	204.9 mAh g^{-1} at 0.5 C, 178.3 mA g^{-1} at 1 C and 154.9 mAh g^{-1} at 2 C.	[14]
15	$Li_{1.2}Mn_{0.53}Ni_{0.13}Fe_{0.13}O_2$ porous	Reverse microemulsion method employing tri-block co-polymer, F068 as a soft-polymer template.	170 mAh g^{-1}-25 mA g^{-1} 100 mAh g^{-1} 206 mA g^{-1}.	[15]
16	$Li_{1.2}Mn_{0.6}Ni_{0.2}O_2$	reverse microemulsion route employing a soft polymer template	240 mA h g^{-1} -25 mA g^{-1} 100 mA h g^{-1}- 500 mA g^{-1}.	[16]

17	Porous $Li_{1.2}Ni_{0.13}Co_{0.13}Mn_{0.54}O_2$	colloidal crystal template assembled by the poly (methyl methacrylate) (PMMA) beads	255 mAh g^{-1} 0.1 C, 140 mAh g^{-1} at 1 C	[17]
18	$Li[Li_{0.2}Ni_{0.2}Mn_{0.6}]O_2$	hydrothermal assisted carbon spheres were used as Templates.	238.7,-1 C, 219.3-2 C 204.8-5 C, 182.7-5 C	[18]
19	$Li_{1.2}Ni_{0.2}Mn_{0.6}O_2$	ordered mesoporous silica (KIT-6) as the hard template	261.2-0.1 C, 225.6-0.2, 214.4-0.5 C, 188.5-1 C 166.9-2 C, 135.4-5 C	[19]
20	$Li_{1.165}Mn_{0.501}Ni_{0.167}Co_{0.167}O_2$	Polymer microsphere-assisted synthesis	231.5-0.1 C, 203.5-0.2 C, 168.2-0.5 C, 144.4-1 C,122.4-2 C, 95.5-5 C, 64.3-10 C	[20]
21	Hollow $0.3Li_2MnO_3{\cdot}0.7LiNi_{0.5}Mn_{0.5}O_2$ microspheres	*In situ* template-sacrificial route	295-15 mA g^{-1}, 271-30 mAh g^{-1} 251-60 mAh g^{-1}, 239-100 mAh g^{-1} 213-200 mAh g^{-1}, 172-500 mAh g^{-1} 125 -1000 mAh g^{-1}	[21]
22	$Li_{1.2}Mn_{0.54}Ni_{0.13}Co_{0.13}O_2$ microrod	Self-template-assisted synthetic	255-0.1 C, 245-0.2 C, 200-0.5 C, 175-1 C 155-2 C, 154-5 C	[22]
23	$Li_{1.2}Ni_{0.2}Mn_{0.6}O_2$ porous microspheres	carbonate co-precipitation and calcination with lithium salt	274-0.1 C, 204-1 C, 179-2 C, 165-3 C 144-5 C	[23]
24	$Li[Li_{0.2}Ni_{0.2}Mn_{0.6}]O_2$ microsphere	Co-precipitation method	280.1 mAh g^{-1} at 0.1 C, 207.1 mAh g^{-1} at 2 C, and 152.4 mAh g^{-1} at 5 C	[24]
25	Porous $0.2Li_2MnO_3{:}0.8LiNi_{0.5}Mn_{0.5}O_2$ nanorods	Self-template - Mn_2O_3 porous nanorods	248 mA h g^{-1}-0.2 C 192 mA h g^{-1}-5 C	[25]
26	$Li_{1.2}Mn_{0.53}Ni_{0.13}Co_{0.13}O_2$, porous, hollow, micro spherical	Hollow MnO_2 as the sacrificial template.	225 mAh g^{-1} - 25 mA g^{-1}, 110 mAh g^{-1} at 1000 mA g^{-1}	[26]

Table S2. Magnetic properties of the pristine and two-week aged (in EC-DMC/$LiPF_6$ solution) Li_2MnO_3 nanostructured samples. Θ_p is the Curie–Weiss temperature; C_p is the Curie constant; μ_{eff} is effective magnetic moment

Samples	C_p (emu·K/mol)	Θ_p (K)	μ_{eff} (μ_B)	Disordered surface layer (mol %)	
				Mn^{3+}	Mn^{2+}
Pristine	1.75	-21.5	3.76	12	7
Aged	1.52	-19.6	3.51	39	23

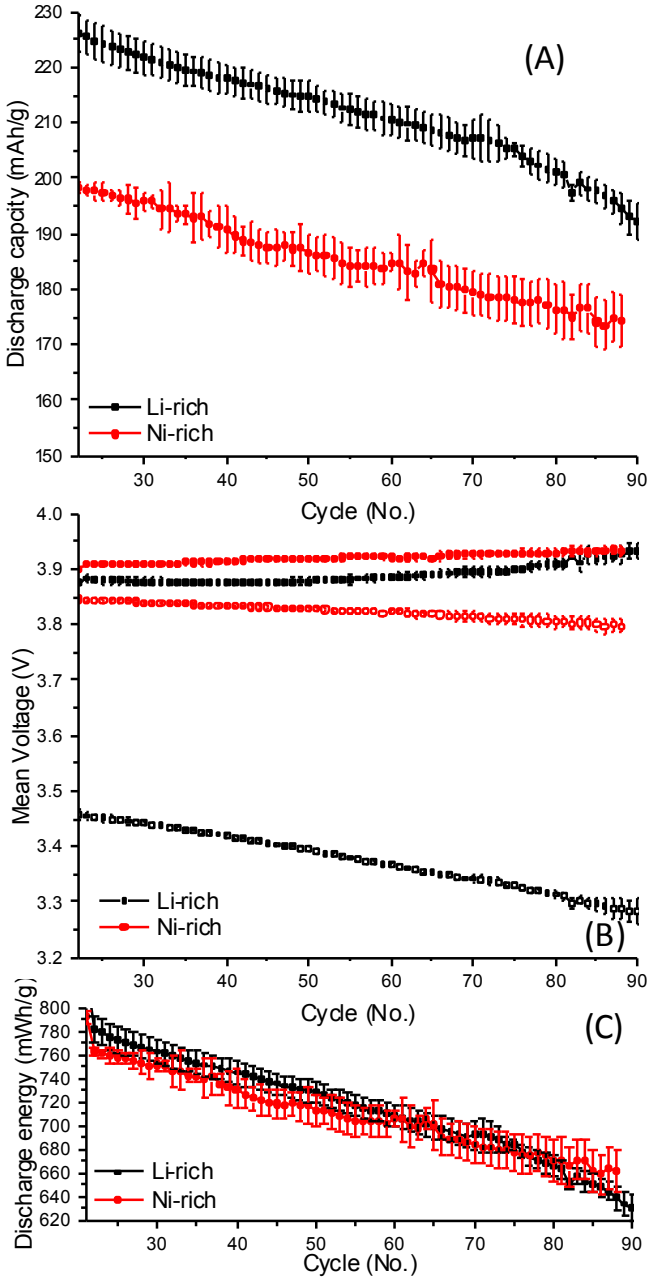

Figure S1 A comparison between the (A) capacity, (B) voltage and (C) energy fade of Ni-rich ($LiNi_{0.8}Co_{0.1}Mn_{0.1}O_2$) and Li- and Mn-rich materials at a C/3 rate (1 C = 180 mAh/g for Ni-rich material). Coin-type cells, with same electrolyte solution and electrode loading. Reprinted from [27]

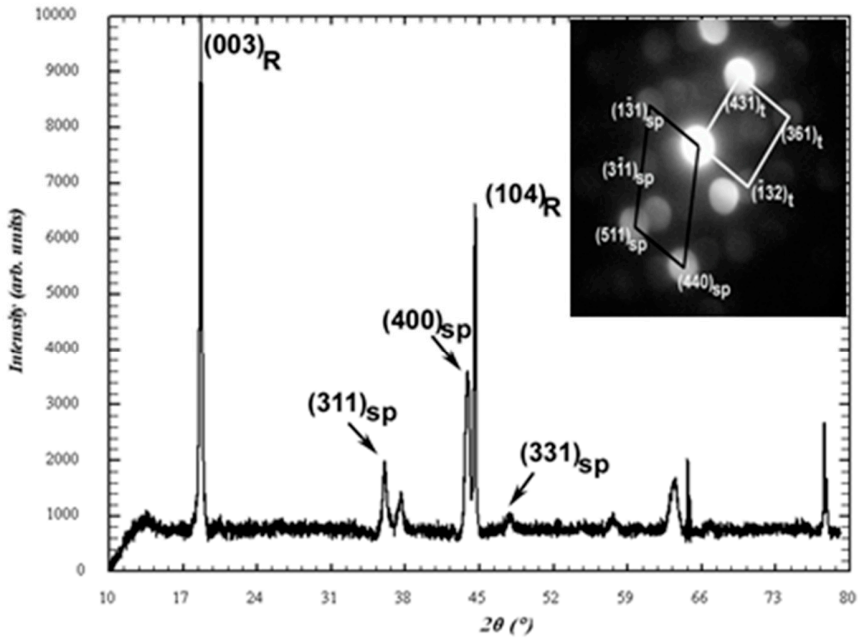

Figure S2 XRD pattern of the cycled $xLi_2MnO_3{\cdot}(1\text{-}x)Li[Mn_yNi_zCo_w]O_2/AlF_3$ material. Labels "R" and "sp" refer, respectively, to the peaks of the rhombohedral and spinel phases. *Insert:* Indexed CBED patterns taken from the cycled $xLi_2MnO_3{\cdot}(1\text{-}x)Li[Mn_yNi_zCo_w]O_2/AlF_3$ material after 40 charge/discharge cycles at 60 °C in a pouch-cell. The patterns demonstrate that in the course of cycling AlF_3 coating of the tetragonal structure is retained. Subscripts "sp" and "t" are related, respectively to spinel phase and tetragonal AlF_3. Reprinted from[28]

Electrodes used in this study (**Figures 1 and S1**) were prepared by loading around 3 mg/cm^2, 80% active material, 10% PVDF, 5% carbon black and 5% graphite *vs.* Li in a coin-type cells using 1.4 M $LiPF_6$ and 3:7 ethylene carbonate to ethyl methyl carbonate solution from BASF. 1 C rate was defined as 250 mAh/g, unless otherwise mentioned.

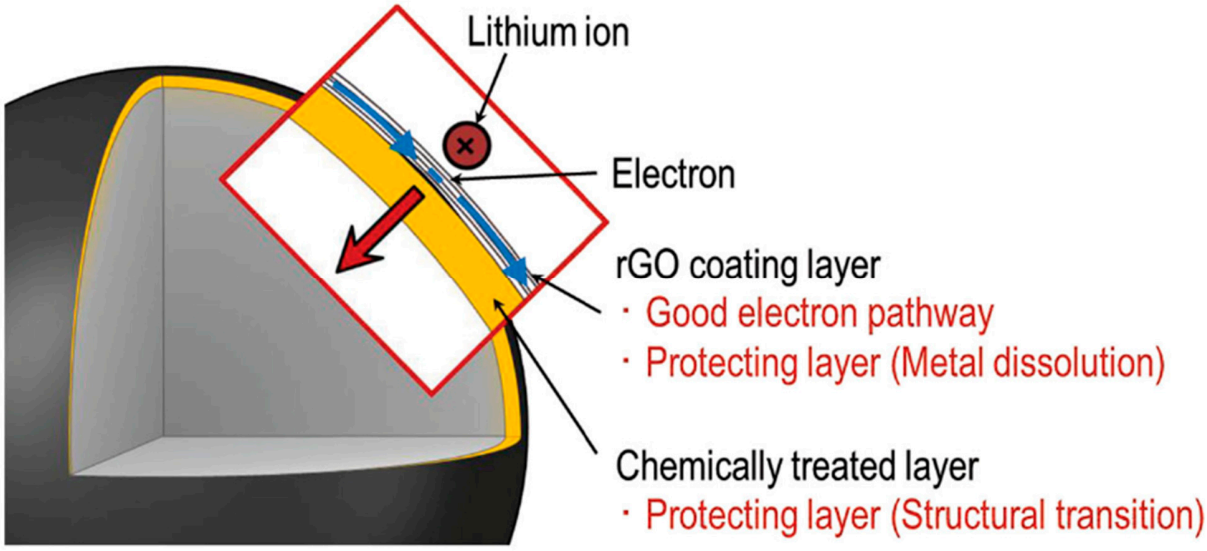

Figure S3 Schematic view of constructing hybrid surface layers consisting of reduced graphene oxide (rGO) and chemically activated phase on cathode materials. Reprinted with permission.[29] Copyright 2014, Wiley-VCH Verlag.

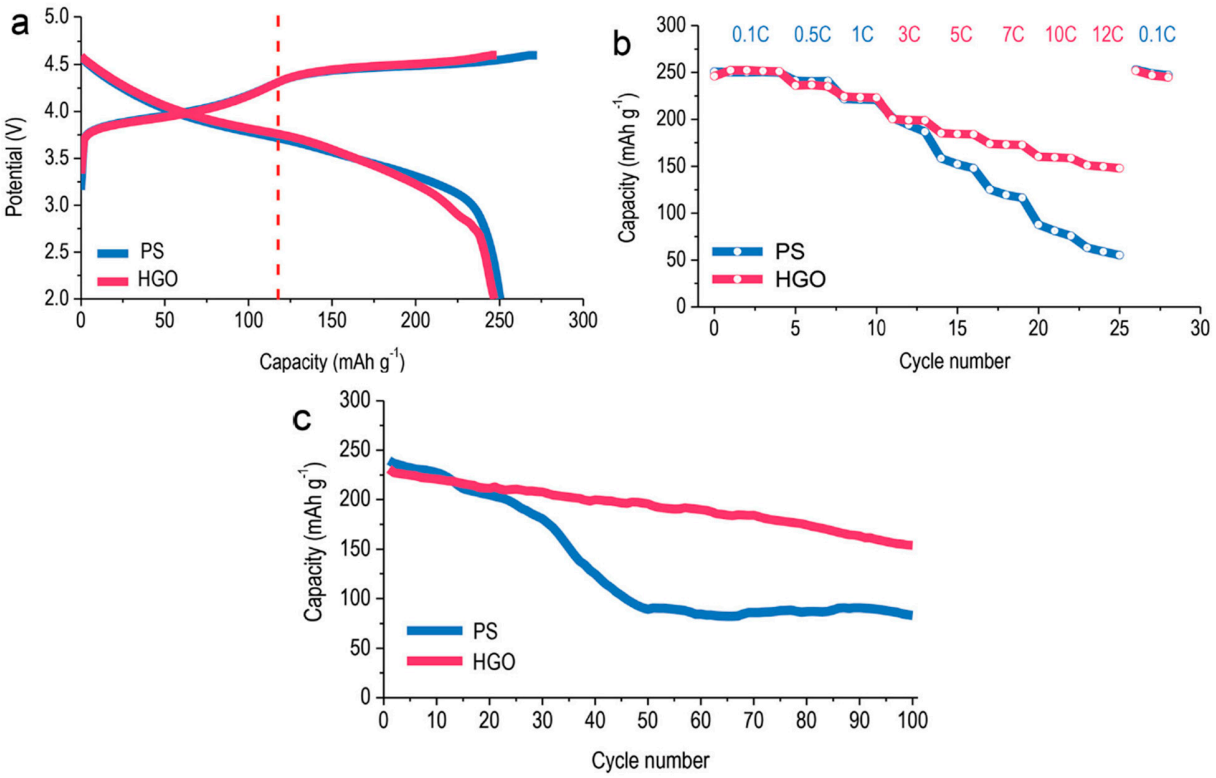

Figure S4 (a) Voltage profiles of PS (pristine sample) and HGO cathodes in coin-type half-cells between 2.0 and 4.6 V at 0.1C rate, at 24 °C. (b) Rate capabilities measured with increasing C-rates from 0.1 to 12 C between 4.6 V and 2.0 V at 24 °C. (c) Cycling performance during 100 cycles between 2.0 and 4.6 V at 1C charge/discharge after initial cycle between 2.0–4.8 V, 0.1 C rate (charge process included constant voltage step). Reprinted with permission.[29] Copyright 2014, Wiley-VCH Verlag.

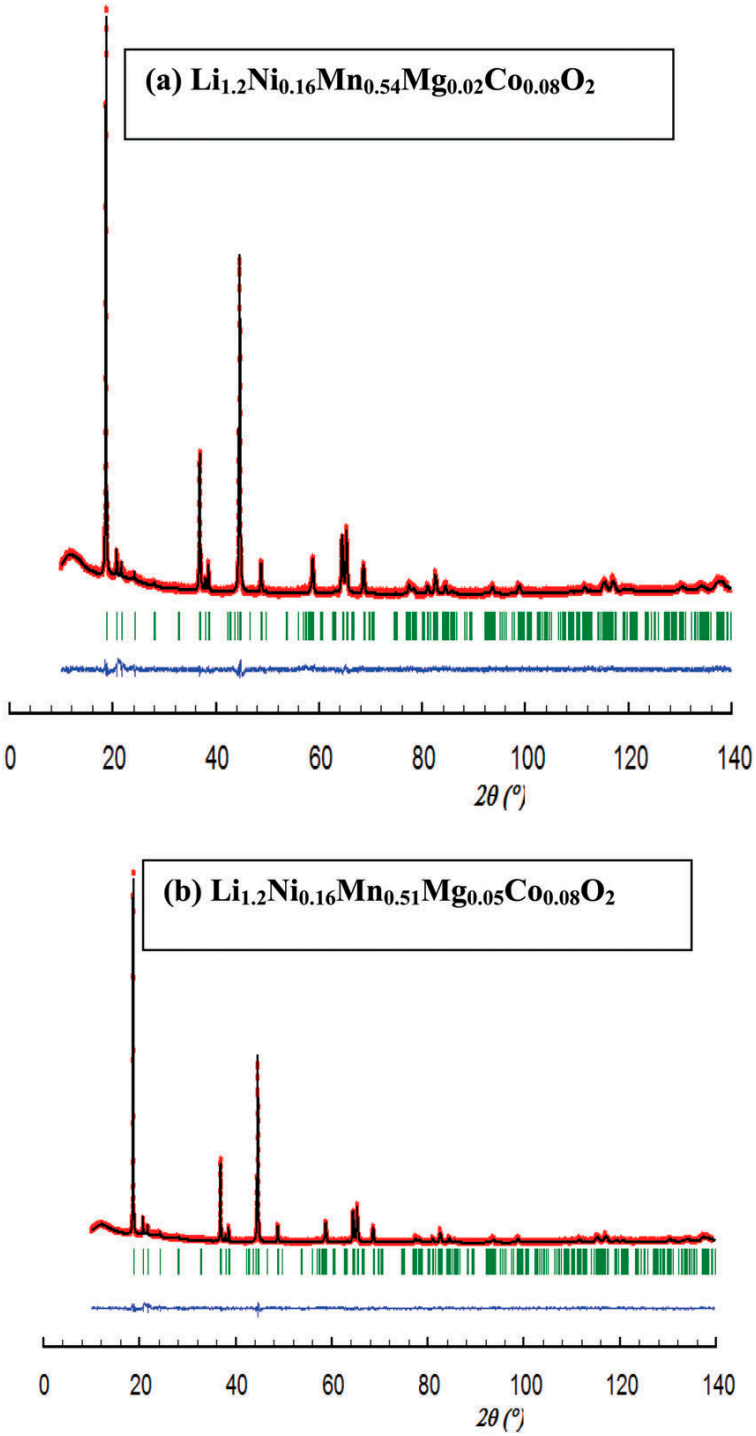

Figure S5 XRD patterns and Rietveld analysis plots of $Li_{1.2}Ni_{0.16}Mn_{0.56-x}Mg_xCo_{0.08}O_2$: (a) x = 0.02, (b) x = 0.05. The calculated patterns are indicated by solid curves; red dots show the observed intensities. The difference between the observed and calculated intensities is indicated

by a blue curve. The short vertical bars indicate the position of Bragg reflections. Reprinted from [30]

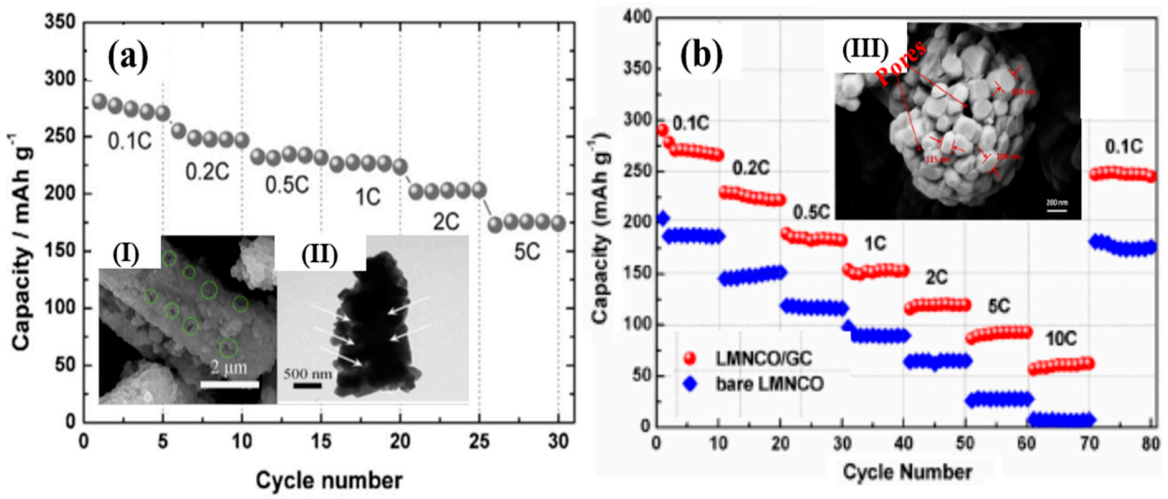

Figure S6 Discharge capacities of (a) electrodes comprising Li,Mn-rich $Li_{1.2}Ni_{0.13}Mn_{0.54}Co_{0.13}O_2$ material prepared by hydrothermal method and (b) $Li_{1.165}Mn_{0.501}Ni_{0.167}Co_{0.167}O_2$ (LMNCO) material prepared by ultrasonic-assisted co-precipitation method, adopting graphene and carbon nanotubes (LMNCO/GC) as functional framework. The cycling was performed under the rates of 0.1 C, 0.2 C, 0.5 C, 1 C, 2 C, 5 C and 10 C, as indicated. FESEM and TEM images (I, II and III) of the above materials are shown in the inset. Reprinted with permission.[1,7] Copyright 2014, Elsevier, and 2016, Royal Society of Chemistry.

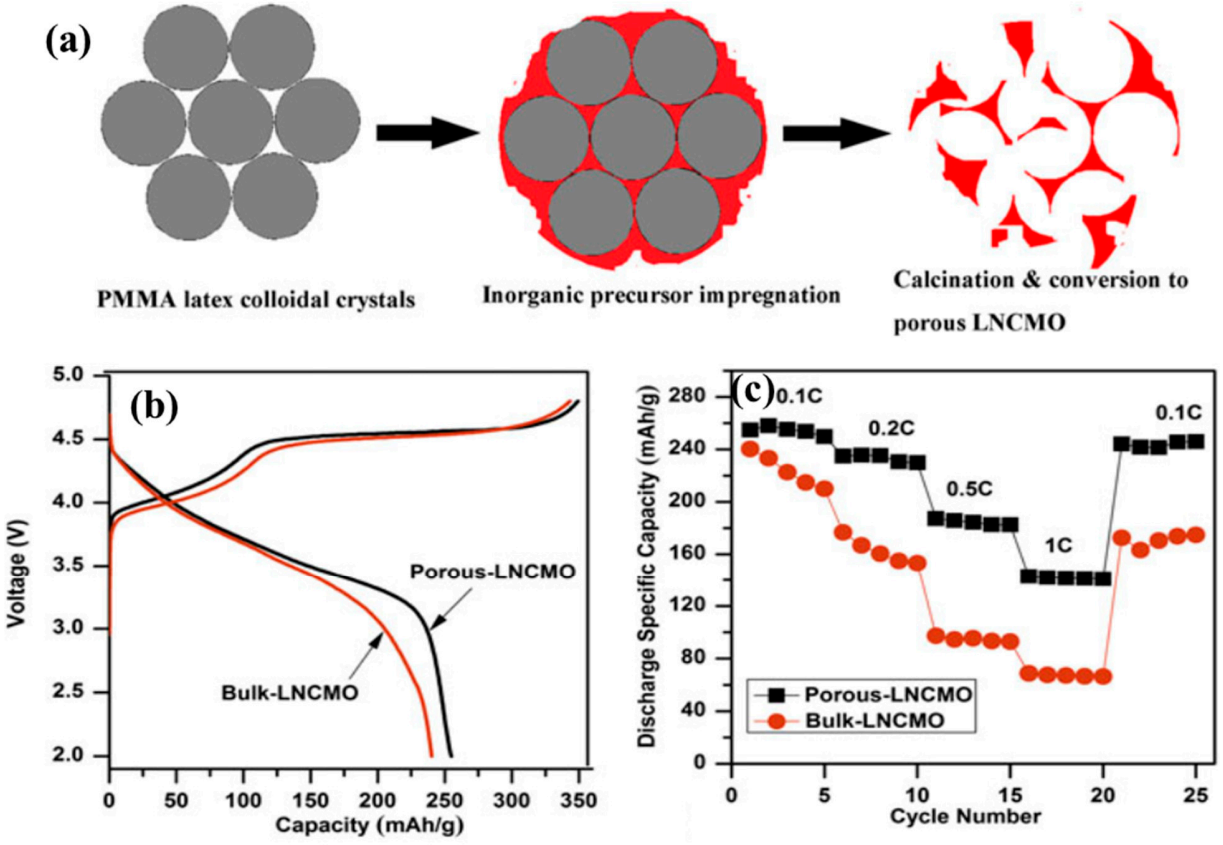

Figure S7 Schematic diagram of the synthesis of porous $Li_{1.2}Ni_{0.13}Co_{0.13}Mn_{0.54}O_2$ (LNCMO) material (a). The initial charge–discharge curves of the first cycle (b) and rate capability of porous $Li_{1.2}Ni_{0.13}Co_{0.13}Mn_{0.54}O_2$ and bulk $Li_{1.2}Ni_{0.13}Co_{0.13}Mn_{0.54}O_2$ electrode materials (c), as indicated. Reprinted with permission.[17] Copyright 2013, the Materials Research Society.

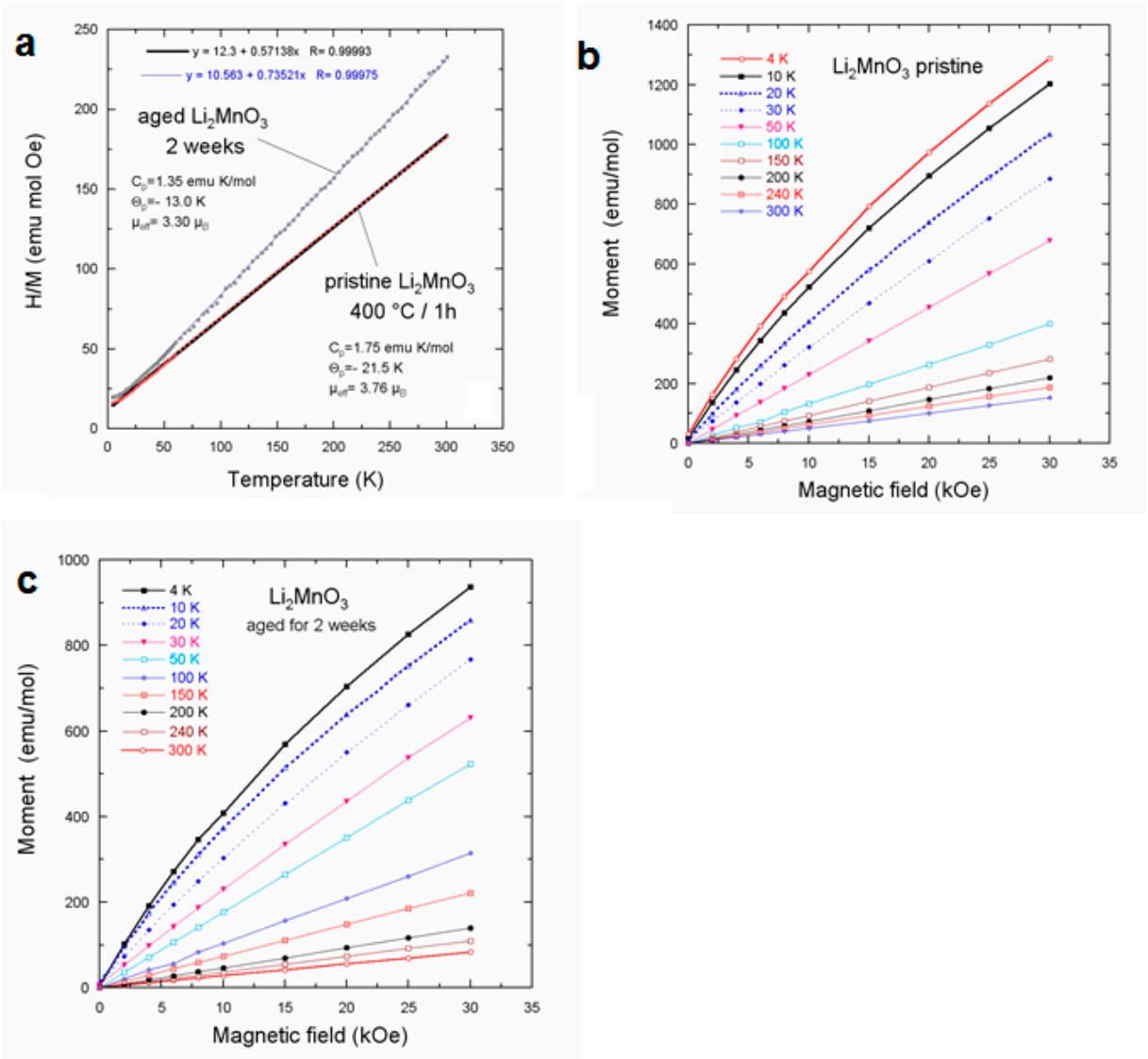

Figure S8 (a) Plot of the reciprocal magnetic susceptibility H/M of the pristine and two-week aged Li_2MnO_3 nanostructured powders. Data were collected with a magnetic field H = 10 kOe. Aging of nano-Li_2MnO_3 material was carried out in EC–DMC/$LiPF_6$ solutions at 60 °C for 2 weeks, in Teflon vials under argon atmosphere, (b) isothermal plots of the magnetization M(H) for pristine and (c) for two-week aged Li_2MnO_3 nanostructured powders. Reprinted with permission.[31] Copyright 2013, Elsevier.

References

1. Zhang, L.; Borong, W.; Ning, L.; Feng, W. Hierarchically porous micro-rod lithium-rich cathode material $Li_{1.2}Ni_{0.13}Mn_{0.54}Co_{0.13}O_2$ for high performance lithium-ion batteries. *Electrochimica Acta* **2014**, *118*, 67-74.
2. Li, Y.; Bai, Y.; Bi, X.; Qian, J.; Ma, L.; Tian, J.; Wu, C.; Wu, F.; Lu, J.; Amine, K. An effectively activated hierarchical nano-/microspherical $Li_{1.2}Ni_{0.2}Mn_{0.6}O_2$ cathode for long-life and high-rate lithium-ion batteries. *ChemSusChem* **2016**.
3. Fu, F.; Wang, Q.; Deng, Y.-P.; Shen, C.-H.; Peng, X.-X.; Huang, L.; Sun, S.-G. Effect of synthetic routes on the rate performance of Li-rich layered $Li_{1.2}Mn_{0.56}Ni_{0.12}Co_{0.12}O_2$. *Journal of Materials Chemistry A* **2015**, *3*, 5197-5203.
4. Fu, F.; Tang, J.; Yao, Y.; Shao, M. Hollow porous hierarchical-structured $0.5Li_2MnO_3{\cdot}0.5LiMn_{0.4}Co_{0.3}Ni_{0.3}O_2$ as a high-performance cathode material for lithium-ion batteries. *ACS Applied Materials & Interfaces* **2016**, *8*, 25654-25659.
5. Luo, K.; Roberts, M.R.; Hao, R.; Guerrini, N.; Liberti, E.; Allen, C.S.; Kirkland, A.I.; Bruce, P.G. One-pot synthesis of lithium-rich cathode material with hierarchical morphology. *Nano Letters* **2016**, *16*, 7503-7508.
6. Li, Y.; Bai, Y.; Wu, C.; Qian, J.; Chen, G.; Liu, L.; Wang, H.; Zhou, X.; Wu, F. Three-dimensional fusiform hierarchical micro/nano $Li_{1.2}Ni_{0.2}Mn_{0.6}O_2$ with a preferred orientation (110) plane as a high energy cathode material for lithium-ion batteries. *Journal of Materials Chemistry A* **2016**, *4*, 5942-5951.
7. Ma, S.; Hou, X.; Li, Y.; Ru, Q.; Hu, S.; Lam, K.-h. Performance and mechanism research of hierarchically structured li-rich cathode materials for advanced lithium–ion batteries. *Journal of Materials Science: Materials in Electronics*, 1-11.
8. Jiang, Y.; Yang, Z.; Luo, W.; Hu, X.-L.; Zhang, W.-X.; Huang, Y.-H. Facile synthesis of mesoporous $0.4Li_2MnO_3{\cdot}0.6LiNi_{2/3}Mn_{1/3}O_2$ foams with superior performance for lithium-ion batteries. *Journal of Materials Chemistry* **2012**, *22*, 14964-14969.
9. Shi, S.; Tu, J.; Tang, Y.; Zhang, Y.; Wang, X.; Gu, C. Preparation and characterization of macroporous $Li_{1.2}Mn_{0.54}Ni_{0.13}Co_{0.13}O_2$ cathode material for lithium-ion batteries via aerogel template. *Journal of Power Sources* **2013**, *240*, 140-148.
10. Penki, T.R.; Shanmughasundaram, D.; Jeyaseelan, A.; Subramani, A.; Munichandraiah, N. Polymer template assisted synthesis of porous $Li_{1.2}Mn_{0.53}Ni_{0.13}Co_{0.13}O_2$ as a high capacity and high rate capability positive electrode material. *Journal of The Electrochemical Society* **2014**, *161*, A33-A39.
11. Penki, T.R.; Shanmughasundaram, D.; Munichandraiah, N. Porous lithium rich $Li_{1.2}Mn_{0.54}Ni_{0.22}Fe_{0.04}O_2$ prepared by microemulsion route as a high capacity and high rate capability positive electrode material. *Electrochimica Acta* **2014**, *143*, 152-160.
12. Chen, D.; Yu, Q.; Xiang, X.; Chen, M.; Chen, Z.; Song, S.; Xiong, L.; Liao, Y.; Xing, L.; Li, W. Porous layered lithium-rich oxide nanorods: Synthesis and performances as cathode of lithium ion battery. *Electrochimica Acta* **2015**, *154*, 83-93.
13. Chen, M.; Xiang, X.; Chen, D.; Liao, Y.; Huang, Q.; Li, W. Polyethylene glycol-assisted synthesis of hierarchically porous layered lithium-rich oxide as cathode of lithium ion battery. *Journal of Power Sources* **2015**, *279*, 197-204.
14. Zhao, C.; Hu, Z.; Qiu, Z.; Liu, K. Urea-assisted combustion synthesis of porous $Li_{1.2}Ni_{0.13}Co_{0.13}Mn_{0.54}O_2$ microspheres as high-performance lithium-ion battery cathodes. *Micro & Nano Letters* **2015**, *10*, 662-665.

15. Penki, T.R.; Shanmughasundaram, D.; Kishore, B.; Jeyaseelan, A.; Subramani, A.; Munichandraiah, N. Composite of li-rich mn, ni and fe oxides as positive electrode materials for Li-ion battery. *Journal of The Electrochemical Society* **2016**, *163*, A1493-A1502.
16. Duraisamy, S.; Penki, T.R.; Nookala, M. Hierarchically porous $Li_{1.2}Mn_{0.6}Ni_{0.2}O_2$ as a high capacity and high rate capability positive electrode material. *New Journal of Chemistry* **2016**, *40*, 1312-1322.
17. Jiang, Y.; Zhuang, H.; Ma, Q.; Jiao, Z.; Zhang, H.; Liu, R.; Chu, Y.; Zhao, B. Synthesis of porous Li_2MnO_3-$LiNi_{1/3}Co_{1/3}Mn_{1/3}O_2$ nanoplates via colloidal crystal template. *Journal of Materials Research* **2013**, *28*, 1505-1511.
18. Zhang, L.; Jiang, J.; Zhang, C.; Wu, B.; Wu, F. High-rate layered lithium-rich cathode nanomaterials for lithium-ion batteries synthesized with the assist of carbon spheres templates. *Journal of Power Sources* **2016**, *331*, 247-257.
19. Li, L.; Wang, L.; Zhang, X.; Xue, Q.; Wei, L.; Wu, F.; Chen, R. 3d-reticular $Li_{1.2}Ni_{0.2}Mn_{0.6}O_2$ cathode material for lithium-ion batteries. *ACS Applied Materials & Interfaces* **2017**.
20. Ma, S.; Hou, X.; Huang, Y.; Li, C.; Hu, S.; Lam, K.-h. Polymer microsphere-assisted synthesis of lithium-rich cathode with improved electrochemical performance. *Ceramics International* **2016**, *42*, 4899-4910.
21. Jiang, Y.; Yang, Z.; Luo, W.; Hu, X.; Huang, Y. Hollow $0.3Li_2MnO_3 \cdot 0.7LiNi_{0.5}Mn_{0.5}O_2$ microspheres as a high-performance cathode material for lithium–ion batteries. *Physical Chemistry Chemical Physics* **2013**, *15*, 2954-2960.
22. Liu, L.; Lu, C.; Xiang, M.; Zhang, Y.; Liu, H.; Wu, H. Template-assisted synthesis of a one-dimensional hierarchical $Li_{1.2}Mn_{0.54}Ni_{0.13}Co_{0.13}O_2$ microrod cathode material for lithium-ion batteries. *ChemElectroChem* **2016**.
23. Ren, W.; Zhao, Y.; Hu, X.; Xia, M. Preparation-microstructure-performance relationship of Li-rich transition metal oxides microspheres as cathode materials for lithium ion batteries. *Electrochimica Acta* **2016**, *191*, 491-499.
24. Li, Y.; Wu, C.; Bai, Y.; Liu, L.; Wang, H.; Wu, F.; Zhang, N.; Zou, Y. Hierarchical mesoporous lithium-rich $Li[Li_{0.2}Ni_{0.2}Mn_{0.6}]O_2$ cathode material synthesized via ice templating for lithium-ion battery. *ACS Applied Materials & Interfaces* **2016**, *8*, 18832-18840.
25. Yang, J.; Cheng, F.; Zhang, X.; Gao, H.; Tao, Z.; Chen, J. Porous $0.2Li_2MnO_3 \cdot 0.8LiNi_{0.5}Mn_{0.5}O_2$ nanorods as cathode materials for lithium-ion batteries. *Journal of Materials Chemistry A* **2014**, *2*, 1636-1640.
26. Duraisamy, S.; Penki, T.R.; Kishore, B.; Barpanda, P.; Nayak, P.K.; Aurbach, D.; Munichandraiah, N. Porous, hollow $Li_{1.2}Mn_{0.53}Ni_{0.13}Co_{0.13}O_2$ microspheres as a positive electrode material for Li-ion batteries. *Journal of Solid State Electrochemistry* **2016**, 1-9.
27. Erickson, E.M.; Schipper, F.; Penki, T.R.; Shin, J.-Y.; Erk, C.; Chesneau, F.-F.; Markovsky, B.; Aurbach, D. Review—recent advances and remaining challenges for lithium ion battery cathodes: Ii. Lithium-rich, xli2mno3·(1-x)liniacobmnco2. *J. Electrochem. Soc.* **2017**, *164*, A6341-A6348.
28. Amalraj, F.; Talianker, M.; Markovsky, B.; Burlaka, L.; Leifer, N.; Goobes, G.; Erickson, E.M.; Haik, O.; Grinblat, J.; Zinigrad, E. Studies of Li and Mn-rich $Li_x[MnNiCo]O_2$ electrodes: Electrochemical performance, structure, and the effect of the aluminum fluoride coating. *Journal of The Electrochemical Society* **2013**, *160*, A2220-A2233.
29. Oh, P.; Ko, M.; Myeong, S.; Kim, Y.; Cho, J. A novel surface treatment method and new insight into discharge voltage deterioration for high-performance $0.4Li_2MnO_3 \cdot 0.6LiNi_{1/3}Co_{1/3}Mn_{1/3}O_2$ cathode materials. *Advanced Energy Materials* **2014**, *4*.

30. Nayak, P.K.; Grinblat, J.; Levi, E.; Levi, M.; Markovsky, B.; Aurbach, D. Understanding the influence of mg doping for the stabilization of capacity and higher discharge voltage of Li- and Mn-rich cathodes for Li-ion batteries. *Physical Chemistry Chemical Physics* **2017**.
31. Amalraj, S.F.; Sharon, D.; Talianker, M.; Julien, C.M.; Burlaka, L.; Lavi, R.; Zhecheva, E.; Markovsky, B.; Zinigrad, E.; Kovacheva, D. Study of the nanosized Li_2MnO_3: Electrochemical behavior, structure, magnetic properties, and vibrational modes. *Electrochimica Acta* **2013**, *97*, 259-270.